공학석사학위논문

# Regression Analysis of Focused Ion Beam Induced Deposition Influenced by Scan Strategies

## 스캔전략에 따른 집속이온빔 적층공정의 회귀분석

**2012년 8월**

서울대학교 대학원

기계항공공학부

김 동 현

**Abstract**

# Regression Analysis of Focused Ion Beam Induced Deposition Influenced by Scan Strategies

Dong-Hyun Kim
School of Mechanical & Aerospace Engineering
The Graduate School
Seoul National University


Focused ion beam (FIB) processing is capable of creating very precious micro and nanoscale structures. This process can remove any solid targets and add several materials, including platinum, carbon and tungsten, and so on. However, it requires the very high cost. So, Many researchers have been attempting to reduce the manufacturing cost by increasing the processing rate by controlling many process parameters, including ion dose, dwell time, and overlap or controlling the ion beam conditions, including ion energy, ion current. In this study, the attempt to increase the processing rate and degree of precision to optimize the FIB processing was implemented by controlling the scan strategy and developing the regression model based on atomic force microscope (AFM) measurement. In this article, the method to predict deposition rate was proposed and its effectiveness was proved through the additional experiments. The regression model was verified with similarity of about 91.1%.

**keywords:** Focused ion beam induced deposition, Deposition rate, Regression analysis, Ion current, Dwell time, Scan strategy

**Student Number : 2010-23203**

# Contents

# List of Tables

# List of Figures

# 1. Introduction

Focused ion beam induced deposition (FIBID) is a powerful technique used for repairing and modification of microelectronics and structuring 3-dimensional nanoscale objects with a high degree of precision [1][2]. This FIBID process may be summarized as follows. Gas molecules are introduced to the sample surface through a gas injector system. By scanning an area with the ion beam, the primary ion beams initiate to dislocate the surface atom, and distributes the excited surface atoms that are contributing to adsorbed gas molecules dissociation. And then, volatile fragment from gas molecules are eliminated by the vacuum system, while the non-volatile components such as carbon, tungsten, and platinum remain fixed on the surface forming a thin film [3][4].

The most commonly used scan strategy for the circuit editing and other applications in FIB is the raster scan strategy that ion beam moves in continuous and discrete ways in *x*-direction (horizontal) and *y*-direction (vertical) respectively [5]. There are several types of scan strategy for FIB processing including serpentine, spiral and circular scan strategies [6]. Each scan strategy can be applied for improving the precision of material processing by reducing the defective nanoscale phenomena such as material redeposition, amorphization [7] and self-focusing [5].

In this study, amorphous carbon ($\alpha$-carbon) structures were deposited on silicon (100) substrate using raster, serpentine, spiral, and offset scan.

Deposition rate was investigated in order to develop prediction model by regression analysis. From regression model, it became able to expect deposition height on individual experiment cases. Also, by AFM measurement, FIBID processing was studied in surface morphologies of carbon deposits for finding out the influences affected by four types of scan strategies.

# 2. Experiments

## 2.1 Deposition rate estimation on processing parameters

The FIBID was carried out using SMI3050, manufactured by SII Nanotechnology. Phenantrhrene ($C_{14}H_{10}$) was used as a precursor gas to deposit α-carbon [8]. The energy of the gallium ion beam was 30 keV, the field of view was 40 μm, ion dose was 5 x $10^{16}$ ions/$cm^2$, dwell times were 1 to 10 μs and ion current was varied from 10 to 90 pA. Detail experimental conditions are shown in Table 2.1.

The four types of scan strategies used are illustrated in Fig. 2.1. As shown in Fig. 2.1. The raster scan includes continuous and discrete process in the *x*- and *y*- directions, and the serpentine scan includes continuous in the *x*- direction (reversely), discrete in *y*- direction. Spiral scan includes continuous in circumferential direction, not proportionally step inside. Offset scan includes continuous in circumferential direction, discrete proportional step inside. In case of the raster and serpentine scan, ion beam moves pixel by pixel with fixed pixel interval passing by the scan area line by line, at the end of each line beam blanking exists. Especially, serpentine scan switches the direction every each scan line. On the other hand, spiral and offset scan have flexible pixel interval with filling up the scan area by unicursal way from outside to inside (or vice versa) [10].

Table 2.1. Experiments conditions of FIBID

| Scan size [μm x μm] | Ion dose [ions/cm$^2$] | Beam size [pA] | Processing time [sec] | Dwell time [μs] | Scan strategy |
|---|---|---|---|---|---|
| 5x5 | 5 x $10^{16}$ | 10 | 200 | 1<br>5<br>10 | Raster<br>Serpentine<br>Spiral<br>Offset |
| | | 30 | 67 | | |
| | | 50 | 40 | | |
| | | 70 | 29 | | |
| | | 90 | 22 | | |

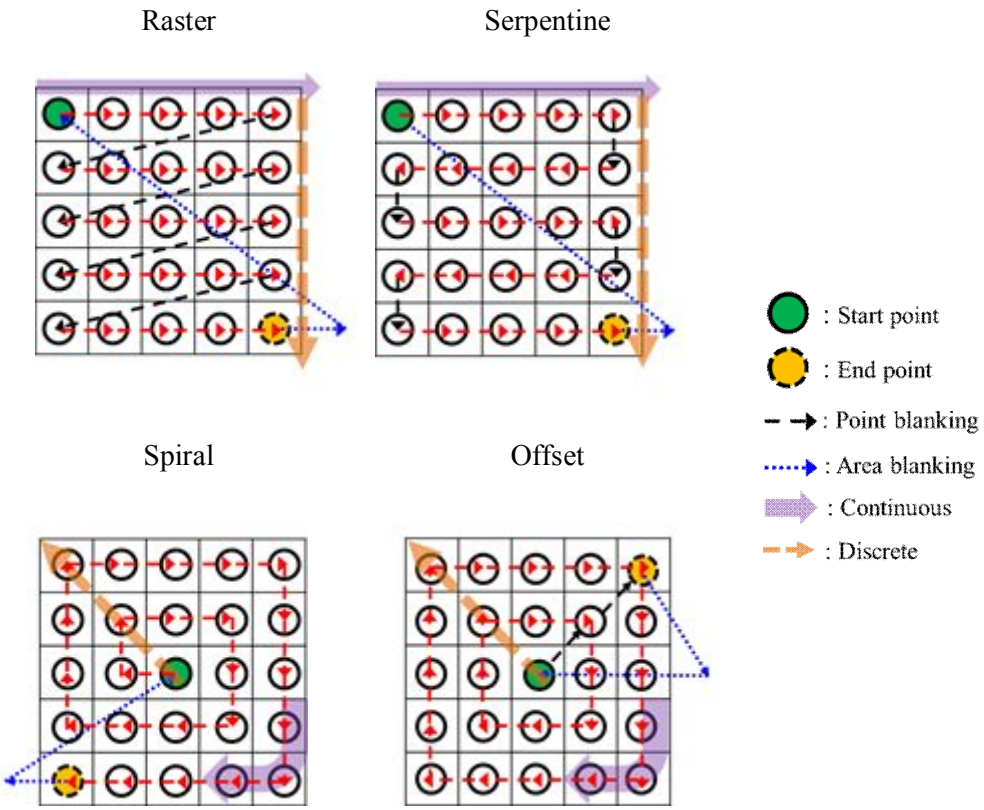


Fig. 2.1. Schematic images of raster, serpentine, spiral, offset scan method

## 2.2 Suitable scan strategy for polygon scanning

The typical scanning method used in FIB applications is the raster scan. The ion beam passes from one side to the other, which is shown in Fig. 2.1. Different scan strategy represents the dissimilar result of degree of precision. Unlike raster and serpentine scan, spiral and offset scan methods have continuous in circumferential direction. Thus, both spiral and offset scan are expected to produce more accurate boundary line. This research investigated by the issue of the influence of beam scan strategy on the boundary accuracy over polygon scanning. The energy of the gallium ion beam was 30 keV, the field of view was 24 μm, ion current was 10 pA, dwell times was 10 μs, scan area was 25 $\mu m^2$, and ion dose was 2 x $10^{16}$ ions/$cm^2$.

# 3. Results and discussion

## 3.1 Regression analysis

There exists several methods that can be used to model manufacturing processes such as mathematical model [9], regression model [10], neural network model [11] and so on. In this paper, the regression analysis was adopted for process modeling in order to expect deposition rate of focused ion beam induced deposition process. The reason why this paper chooses regression analysis is that it can verify both functional attributes and capabilities of each parameter.

Table 3.1. Deposition rate FIBID of carbon

| Ion current [pA] | Scan strategy | Deposition rate [nm/sec] | | | | | |
|---|---|---|---|---|---|---|---|
| | | 1st experiment | | | 2nd experiment | | |
| | | Dwell time [ms] | | | | | |
| | | 1 | 5 | 10 | 1 | 5 | 10 |
| 10 | Raster | 0.698 | 0.584 | 0.458 | 1.162 | 0.707 | 0.570 |
| | Serpentine | 0.803 | 0.535 | 0.470 | 1.148 | 0.647 | 0.597 |
| | Spiral | 0.732 | 0.591 | 0.560 | 0.862 | 0.651 | 0.690 |
| | Offset | 0.787 | 0.590 | 0.505 | 1.197 | 0.688 | 0.639 |
| 30 | Raster | 0.939 | 1.173 | 1.092 | 1.394 | 1.341 | 1.508 |
| | Serpentine | 0.956 | 1.192 | 0.920 | 1.497 | 1.440 | 1.224 |
| | Spiral | 0.949 | 1.367 | 1.062 | 1.523 | 1.676 | 1.287 |
| | Offset | 0.977 | 1.452 | 1.059 | 1.640 | 1.622 | 1.284 |
| 50 | Raster | 1.587 | 1.529 | 1.187 | 2.492 | 2.022 | 1.660 |
| | Serpentine | 1.582 | 1.443 | 1.227 | 2.525 | 1.994 | 1.740 |
| | Spiral | 1.572 | 1.747 | 1.487 | 2.102 | 2.141 | 2.109 |
| | Offset | 1.621 | 1.881 | 1.469 | 2.406 | 2.268 | 1.944 |
| 70 | Raster | 2.042 | 1.744 | 1.413 | 3.100 | 2.106 | 2.154 |
| | Serpentine | 1.966 | 1.605 | 1.442 | 2.604 | 2.049 | 1.996 |
| | Spiral | 2.034 | 2.318 | 1.846 | 2.905 | 2.456 | 2.531 |
| | Offset | 2.142 | 2.417 | 1.584 | 2.914 | 2.830 | 2.280 |
| 90 | Raster | 2.997 | 2.147 | 1.455 | 4.931 | 2.959 | 2.521 |
| | Serpentine | 2.739 | 1.926 | 1.347 | 5.650 | 3.112 | 2.270 |
| | Spiral | 3.041 | 2.410 | 1.793 | 5.272 | 2.949 | 2.788 |
| | Offset | 3.125 | 2.489 | 1.945 | 4.431 | 2.968 | 2.556 |

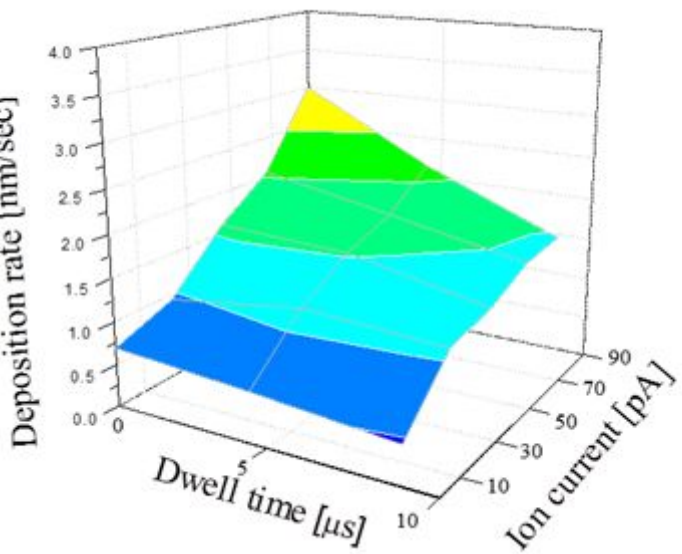


Fig. 3.1. Deposition rate FIBID of carbon in raster scan

Table 3.1 and Fig. 3.1 showed the deposition rate calculated from the dimensoional data by AFM measurement. Figure 3.1 represented the deposition rate in case of raster scan. Based on structure height and processing time, deposition rate was calculated. Different types of regression models dependent on the order and nonlinearity of variables were developed. In this work, polynomial multiple regression model was proposed to estimate deposition rate. Using stepwise regression analysis to remove invalid term, the final regression model to predict deposition rate was given below.

$$y = \beta_0 + \beta_1 x_1 + \beta_2 x_1^2 x_2 \qquad (1)$$

In equations (1) $x_1$ and $x_2$ are input variables that represent ion current [pA], dwell time [μs] respectively. Output variable $y$ is the value of the estimated deposition rate [nm/s]. Then, statistics from the developed model coefficient of Eq. (1) are presented in Table 3.2.

Table 3.2. Coefficients for regression model

| | $\beta_0$ | $\beta_1$ | $\beta_2$ |
|---|---|---|---|
| Raster | 0.263 | 0.0377 | - 0.000023 |
| Serpentine | 0.208 | 0.0383 | - 0.000025 |
| Spiral | 0.247 | 0.0383 | - 0.000018 |
| Offset | 0.345 | 0.0366 | - 0.000018 |

Table 3.3. ANOVA and summaries of the regression models

| Scan style | Source | Degree of Freedom | Sum of square | Mean square | $F_0$ | P-value prob > F |
|---|---|---|---|---|---|---|
| Raster | Regression | 2 | 19.9761 | 9.988 | 44.56 | 0 |
| | Residual Error | 27 | 6.0521 | 0.2242 | | |
| | Lack of fit | 12 | 1.4154 | 0.1179 | 0.38 | 0.95 |
| | Pure error | 15 | 4.6367 | 0.3091 | | |
| | Total | 29 | 26.0282 | | | |
| | | | ( $R^2$=76.7%, $R^2$(adj)=75.0%) | | | |
| Serpentine | Regression | 2 | 20.204 | 10.102 | 29.42 | 0 |
| | Residual Error | 27 | 9.272 | 0.343 | | |
| | Lack of fit | 12 | 2.427 | 0.202 | 0.44 | 0.919 |
| | Pure error | 15 | 6.846 | 0.456 | | |
| | Total | 29 | 29.476 | | | |
| | | | ( $R^2$=68.5%, $R^2$(adj)=66.2%) | | | |
| Spiral | Regression | 2 | 22.517 | 11.259 | 50.44 | 0 |
| | Residual Error | 27 | 6.027 | 0.223 | | |
| | Lack of fit | 12 | 1.606 | 0.134 | 0.45 | 0.913 |
| | Pure error | 15 | 4.421 | 0.295 | | |
| | Total | 29 | 28.544 | | | |
| | | | ( $R^2$=78.9%, $R^2$(adj)=77.3%) | | | |
| Offset | Regression | 2 | 20.15 | 10.075 | 78.3 | 0 |
| | Residual Error | 27 | 3.474 | 0.129 | | |
| | Lack of fit | 12 | 0.842 | 0.07 | 0.4 | 0.942 |
| | Pure error | 15 | 2.632 | 0.175 | | |
| | Total | 29 | 23.624 | | | |
| | | | ( $R^2$=85.3%, $R^2$(adj)=84.2%) | | | |

Generally, the precision of the regression model can be tested using analysis of variance (ANOVA) technique. The coefficient of determination, $R^2$ is used to find how closely the predicted and experimental value lies on. The value of $R^2$ for the above -developed relationship is also presented in table 3.3. The adjusted $R^2$ were 0.68~0.85, showing that 68~80% of the observed variability in deposition rate could be explained by the independent variable. Larger values of $R^2$ suggested models of greater predictive ability. The precision of the regression model improved as the $F_0$ value became larger. Table 3.3 shows that "prob>F" less than 0.05 indicate regression model is valid. Furthermore, The lack of fit data indicates regression model is reasonable

Table 3.4. Model verifying experiment design and results

| Scan strategy | Ion current [pA] | Dwell time [μs] | Expect thickness [nm] | Actual thickness [nm] | Error [%] |
|---|---|---|---|---|---|
| Raster | 40 | 5 | 78 | 86 | 9.30 |
| | 40 | 20 | 50.4 | 57 | 11.57 |
| | 200 | 5 | 31.76 | 28.7 | -10.66 |
| Serpentine | 40 | 5 | 77 | 81.1 | 5.05 |
| | 40 | 20 | 47 | 52.15 | 9.87 |
| | 200 | 5 | 28.68 | 29.1 | 1.44 |
| Spiral | 40 | 5 | 81.75 | 93.7 | 12.75 |
| | 40 | 20 | 60.15 | 58.57 | -2.69 |
| | 200 | 5 | 43.07 | 48.7 | 11.56 |
| Offset | 40 | 5 | 83.25 | 94.9 | 12.27 |
| | 40 | 20 | 61.62 | 57.9 | -6.47 |
| | 200 | 5 | 40.65 | 46.9 | 13.32 |

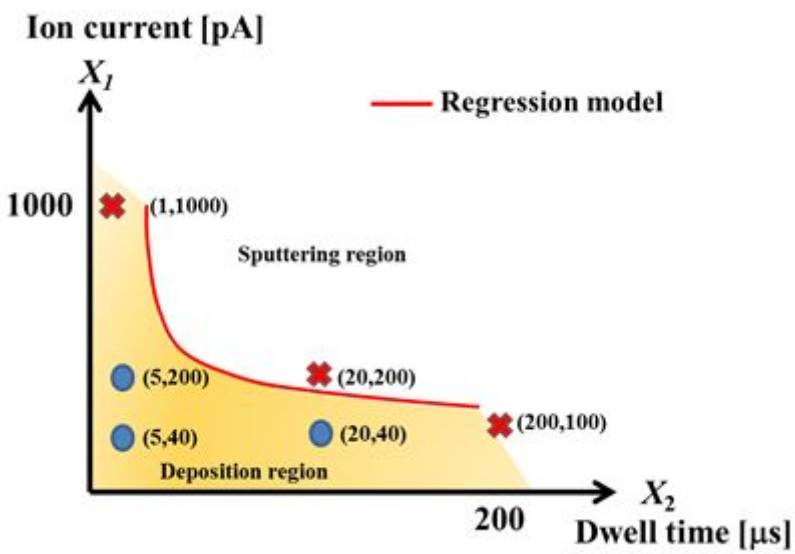


Fig. 3.2. Transition boundary between sputtering and deposition

To verify prediction models, deposition experiments using three different experiment conditions for each scan strategy were implemented. The regression model graph represented average coefficient value model due to similarity of four types of scan strategies. By utilizing the dwell time of 5 and 20 μs and the ion current of 40 and 200 pA, detailed experiment conditions and prediction results were listed in Table 3.4. Each experimental condition was determined from interpolation and extrapolation. As a result, average percentage deviation of the regression model was 8.9%. Fig 3.2 showed transition boundary between sputtering and deposition. Regression model is not reasonable when it comes to breaking the bounds of 200 μs and 1000 pA. Also, in case of experimental condition at above the line, regression model is not suitable. Since, sputtering event is dominant role of process than deposition.

## 3.2 Effects of factors on deposition rate

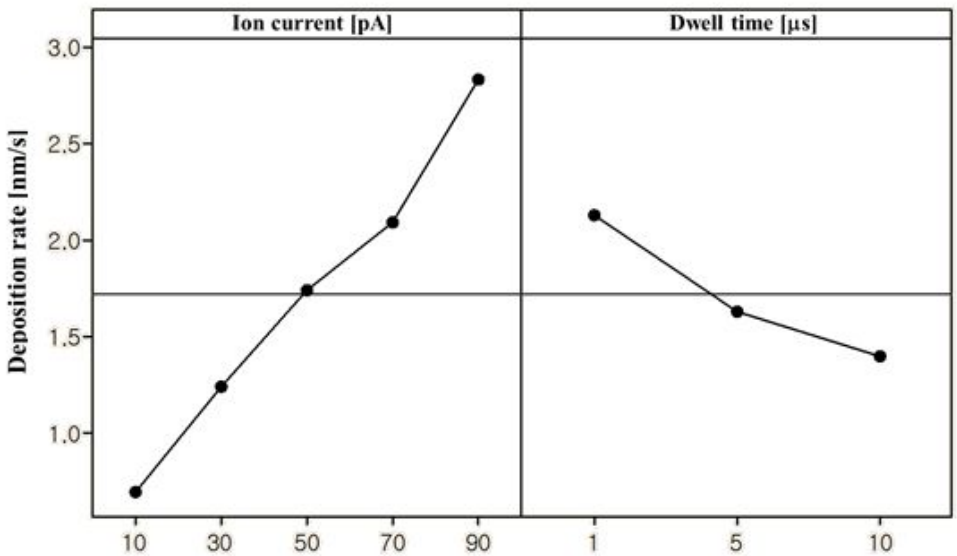


Fig. 3.3. Plot of main effects on deposition rate

The plot of main effects of factors can be used to draw out a conclusion about effects of factors. This plot is shown in Fig. 3.3. Figure 3.3 explains that the deposition rate is decreased by increasing the dwell time. On the contrary increasing the ion current, deposition rate is increased. Because the deposition process is governed by three processes related to the absorption of precursor gas onto the substrate, the decomposition by excited surface atoms and the sputtering of newly deposited products by primary ion beam [2]. As shown in Table 1.1, experiment condition, gas feed rate is sufficient to deposition process with 10 to 90 pA ion current. However, gas feed rate is insufficient for decomposing to deposition process with 1 to 10 μs dwell time. Hence, deposition takes small portion of deposition process as increasing the dwell time. Consequently, deposition rate diminishes gradually. This plot shows that slope of ion current is greater than that of dwell time. It means that deposition rate is more sensitive to variation of ion current than that of dwell time. Regulating ion current is highly efficient in manufacturability with equivalent effect on deposition rate. In other words, it is useful to increasing the ion current ten times that reducing a tenth part of dwell time.

## 3.3 Surface morphologies of α-carbon

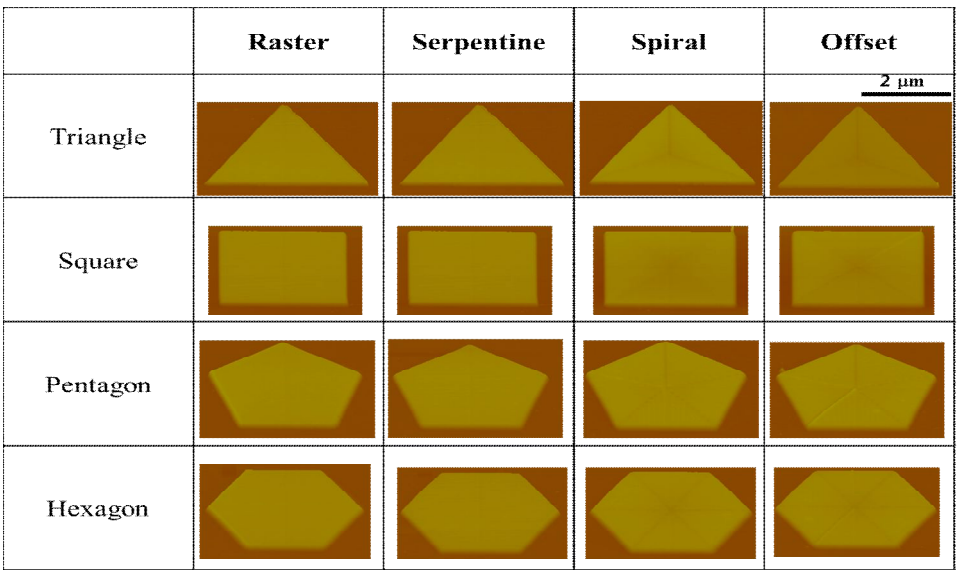


Fig. 3.4. AFM images of α-carbon according to 4 types of scan strategies

Figure 3.4 shows the surface morphology of the FIBID structures by The AFM. To observe the morphology of the FIBID products, atomic force microscope (AFM, dimension 3100, Veeco) were used. The AFM was applied for measuring the height of the deposited structures. Because the most important parameters for calculating deposition rate was height. Width and height length of deposited structures were measured from distances on both ends of bottom plane in AFM profile line. The data for each condition was made by more than twice AFM measurements to minimize dimensional errors.

| | Raster | Serpentine | Spiral | Offset |
|---|---|---|---|---|
| Triangle | 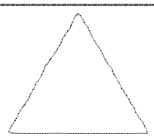 | 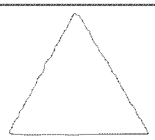 | 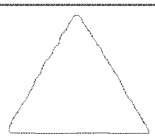 | 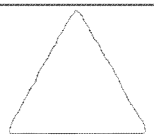 |
| Square |  |  |  |  |
| Pentagon | 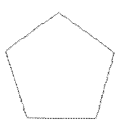 | 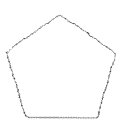 | 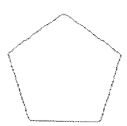 | 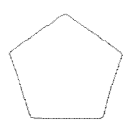 |
| Hexagon | 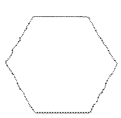 | 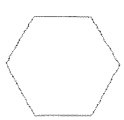 |  | 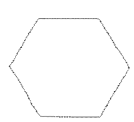 |

Fig. 3.5. Boundary lines of α-carbon

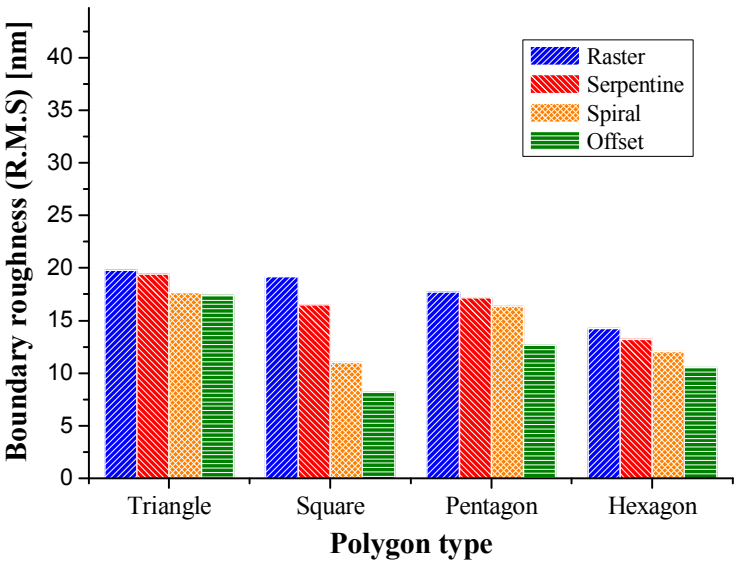


Fig. 3.6. Line edge roughness of α-carbon

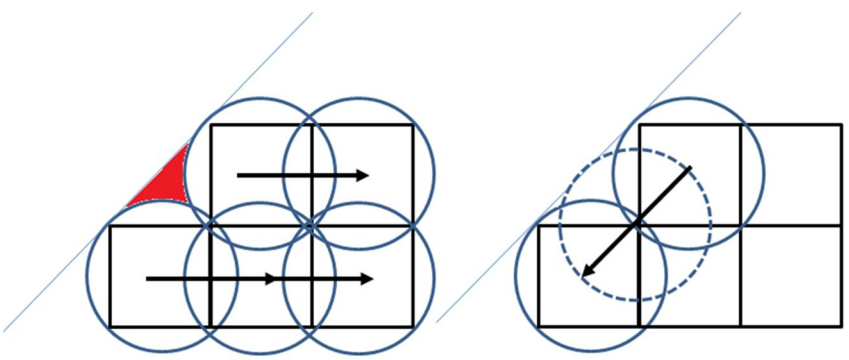

Raster, Serpentine scan Spiral, Offset scan

Fig. 3.7. Boundary line margin error by scan strategy

Figure 3.5 showed the boundary line of the FIBID structures from AFM images. To calculate the line edge roughness, extracting actual boundary line is used on root mean square (R.M.S). As shown in Fig. 3.6 spiral and offset scan method showed the enhanced boundary accuracy. Since, It is related to paths on inclined line. In case of raster, serpentine scan method, these two method generate margin because of the difference between pixel and beam shape in Fig. 3.7. In contrast, spiral and offset scan do not make margin at inclined line. For these reasons, as increasing the ratio of inclined line over all the lines of polygon, spiral and offset scan give better boundary accuracy.

# 4. Conclusions

A regression model to predict focused ion beam induced deposition rate was developed in this paper. The procedure for experiment is summarized as follows. Under the same conditions of ion dose, scan size and precursor gas, experiments change the dwell time and ion current condition with different scan strategy such as raster, serpentine, spiral and offset scan. Then, the cross-sectional profiles was measured by AFM. Deposition rate was predicted from the experimental results by AFM measurement. The polynomial multiple regression model was proposed and its effectiveness was verified from additional experiments. Prediction model had prediction accuracy of about 91%. Results showed that the developed deposition rate model could accurately predict the deposition rate of focused ion beam induced deposition process.

It has been observed that the deposition rate is higher as the ion current in increased. However, deposition rate is gradually reduced with increasing dwell time. Deposition rate is more sensitive to variation of ion current than that of dwell time based on main effects plot. four types of scan strategies do not make a clear the difference at deposition rate. But the Spiral and offset scan method showed the enhanced boundary accuracy. This leads to the fact that scan strategy methodology research should be encouraged. To enhance the modeling capability and reliability, more experiment with various conditions should be encouraged.

# Bibliography

[1] Kim, C.S., Ahn, S.H., Jang, D.Y., 2012. Review: Developments in Micro/Nanoscale Fabrication by Focused ion beams. Vacuum. 86, 1014–1035.

[2] Fu, Y., Bryan, N.K.A., Shing, O.N., 2001. Characterization of focused ion beam induced deposition process and parameters calibration. Sensors and actuators A 88, 58-66.

[3] Hopman, W.C.L., Ay, F., Hu, W., Gadgil, V.J., Kuipers, L., Pollanu, M. and Ridder, R.M.d., 2007. Focused ion beam scan routine, dwell time and dose optimizations for submicrometre period planar photonic crystal components and stamps in silicon. Nanotechnology. 18. 195305.

[4] Utke I, Hoffmann P, Melngailis J., 2008. Gas-assisted focused electron beam and ion beam processing and fabrication. J. Vac. Sci. Technol. B. 26, 1197-1276.

[5] Nellen, P.M. and Br¨onnimann, R., 2006. Meas. Sci. Technol. 17, 943-948.

[6] Steckl, A.J. and Chyr, I., 1999, Focused ion beam micromilling of GaN and related substrate materials sapphire, SiC, and Si. J. Vac. Sci. Technol. B 17(2), 362-365.

[7] Rajsiri, S., Kempshall, B. W., Schwarz, S.M. and Giannuzzi, L.A., 2002. FIB Damage in Silicon : Amorphization or Redeposition ?. Microsc. Microanal. 8, 50-51.

[8] Voevodin, a. a., Capano, M. a., Safriet, a. J., Donley, M.S. & Zabinski, J.S., 1996. Combined magnetron sputtering and pulsed laser deposition of carbides and diamond-like carbon films. Applied Physics Letters 69, 188-190.

[9] Ready, J.F. and Farson, D.F., 2001. LIA Handbook of laser material processing, Laser Institute of America. pp. 167-204.

[10] Park, H.S. and Rhee, S.H., 1999. Estimation of weld bead size in CO2 laser welding by using multiple regression and neural network , J. Laser Appl. 11. 143-150.

[11] Salminen, A.S., 2001. Effect of Welding Parameters on the Efficiency and Energy Distribution during Laser Welding with Filler Wire, Proc. of ICALEO, Section C, 1704-1707.

[12] Kim, C.S., Kim, H.J., Jang, D.Y., Ahn, S.H., 2010. Morphological influence of the beam overlap in focused ion beam induced deposition using raster scan. Microelectron. Eng. 87, 972-976.

[13] Kim, C.S., Ahn, S.H., Jang, D.Y., 2010. Nanoscale Effects in Carbon Structures Fabricated using Focused Ion Beam - Chemical Vapor Deposition. Thin Solid Films. 518, 5177-5182.

[14] Yasaka, A., Aramaki, F., Muramatsu, M., Kozakai,T., Matsuda,O., Sugiyama, Y., Doi, T., Takaoka, O., Hagiwara, R. and Kakamae, K., 2008. Application of vector scanning in focused ion beam photomask repair system, J. Vac. Sci. Technol. B 26 (6), 2127-2130.

[15] Chong, E.K.P. and Zak, S.H., 2001. An introduction to optimization, John Wiley & Sons, Inc. pp. 113-122.

[16] Tseng,A.a., Insua,I.A., Park, J.S. and Chen, C.D., 2005. Milling yield estimation in focused ion beam milling of two-layer substrates , J. Micromech. Microeng. 15 20-28.

[17] Padmanaban, G., Balasubramanian, V., 2010. Optimization of laser beam welding process parameters to attain maximum tensile strength in AZ31B magnesium alloy , Optics & Laser Technology, 42, 1253–1260.

[18] Hoseinpour Golloa, M., Mahdavianb, S.M., Moslemi Naeini, H., 2011. Statistical analysis of parameter effects on bending angle in laser forming process by pulsed Nd:YAG laser, Optics & Laser Technology, 43, 475–482.

[19] Kim, T.W and Park, Y.W., 2011. Parameter optimization using a regression model and fitness function in laser welding of aluminum alloys for car bodies , INTERNATIONAL JOURNAL OF PRECISION ENGINEERING AND MANUFACTURING, 12, 313-320.

[20] Chang, H.K, Kim, J.H, Kim, H.I, Jang, D.Y, Han, D.C., 2007. In-process surface roughness prediction using displacement signals from spindle motion, International Journal of Machine Tools and Manufacture, 47, 1021–1026.

[21] Frey, L., Lehrer, C., Ryssel, H., 2003. Nanoscale effects in focused ion beam processing. Appl. Phys. A 76,1017-1023.

# 요약(국문초록)

집속이온빔 공정은 나노 마이크로 스케일에서 매우 정밀한 구조를 만들 수 있는 공정이다. 본 공정은 다양한 물질을 제거할 수 있고 가스분자를 시료 표면에 분사하여 플래티늄, 탄소, 텅스텐 등을 적층할 수 있다. 그러나 공정비용이 매우 고가이다. 많은 연구자들이 이온 도즈, 드웰 타임, 빔 오버랩과 같은 다양한 공정변수를 조절하고 이온에너지, 이온전류와 같은 이온빔 변수를 조절해서 공정 수율을 최적화를 통해 공정비용을 줄이려 노력하고 있다. 본 연구에서는, 집속이온빔 공정의 공정 수율 증가와 가공 정밀도 향상을 위해 스캔전략을 제어하고 회귀분석 모델을 구현하는 연구를 진행하였다. 본 논문에서는 증착 수율을 예측할 수 있는 방법을 제안하고 추가실험을 통해 검증하였다. 회귀분석 모델의 정확도는 91.1%이다.

**주요어 : Focused ion beam deposition, Deposition rate, Regression analysis, Ion current, Dwell time, Scan strategy**

**학 번 : 2010-23203**